

International Journal of Physical Sciences

Volume 11 Number 8 30 April , 2016

ISSN 1992-1950



*Academic
Journals*

ABOUT IJPS

The **International Journal of Physical Sciences (IJPS)** is published weekly (one volume per year) by Academic Journals.

International Journal of Physical Sciences (IJPS) is an open access journal that publishes high-quality solicited and unsolicited articles, in English, in all Physics and chemistry including artificial intelligence, neural processing, nuclear and particle physics, geophysics, physics in medicine and biology, plasma physics, semiconductor science and technology, wireless and optical communications, materials science, energy and fuels, environmental science and technology, combinatorial chemistry, natural products, molecular therapeutics, geochemistry, cement and concrete research, metallurgy, crystallography and computer-aided materials design. All articles published in IJPS are peer-reviewed.

Contact Us

Editorial Office: ijps@academicjournals.org

Help Desk: helpdesk@academicjournals.org

Website: <http://www.academicjournals.org/journal/IJPS>

Submit manuscript online <http://ms.academicjournals.me/>

Editors

Prof. Sanjay Misra

*Department of Computer Engineering, School of Information and Communication Technology
Federal University of Technology, Minna,
Nigeria.*

Prof. Songjun Li

*School of Materials Science and Engineering,
Jiangsu University,
Zhenjiang,
China*

Dr. G. Suresh Kumar

*Senior Scientist and Head Biophysical Chemistry
Division Indian Institute of Chemical Biology
(IICB)(CSIR, Govt. of India),
Kolkata 700 032,
INDIA.*

Dr. Remi Adewumi Oluayinka

*Senior Lecturer,
School of Computer Science
Westville Campus
University of KwaZulu-Natal
Private Bag X54001
Durban 4000
South Africa.*

Prof. Hyo Choi

*Graduate School
Gangneung-Wonju National University
Gangneung,
Gangwondo 210-702, Korea*

Prof. Kui Yu Zhang

*Laboratoire de Microscopies et d'Etude de
Nanostructures (LMEN)
Département de Physique, Université de Reims,
B.P. 1039. 51687,
Reims cedex,
France.*

Prof. R. Vittal

*Research Professor,
Department of Chemistry and Molecular
Engineering
Korea University, Seoul 136-701,
Korea.*

Prof Mohamed Bououdina

*Director of the Nanotechnology Centre
University of Bahrain
PO Box 32038,
Kingdom of Bahrain*

Prof. Geoffrey Mitchell

*School of Mathematics,
Meteorology and Physics
Centre for Advanced Microscopy
University of Reading Whiteknights,
Reading RG6 6AF
United Kingdom.*

Prof. Xiao-Li Yang

*School of Civil Engineering,
Central South University,
Hunan 410075,
China*

Dr. Sushil Kumar

*Geophysics Group,
Wadia Institute of Himalayan Geology,
P.B. No. 74 Dehra Dun - 248001(UC)
India.*

Prof. Suleyman KORKUT

*Duzce University
Faculty of Forestry
Department of Forest Industrial Engineering
Beciyorukler Campus 81620
Duzce-Turkey*

Prof. Nazmul Islam

*Department of Basic Sciences &
Humanities/Chemistry,
Techno Global-Balurghat, Mangalpur, Near District
Jail P.O: Beltalpark, P.S: Balurghat, Dist.: South
Dinajpur,
Pin: 733103,India.*

Prof. Dr. Ismail Musirin

*Centre for Electrical Power Engineering Studies
(CEPES), Faculty of Electrical Engineering, Universiti
Teknologi Mara,
40450 Shah Alam,
Selangor, Malaysia*

Prof. Mohamed A. Amr

*Nuclear Physic Department, Atomic Energy Authority
Cairo 13759,
Egypt.*

Dr. Armin Shams

*Artificial Intelligence Group,
Computer Science Department,
The University of Manchester.*

Editorial Board

Prof. Salah M. El-Sayed

*Mathematics. Department of Scientific Computing,
Faculty of Computers and Informatics,
Benha University. Benha ,
Egypt.*

Dr. Rowdra Ghatak

*Associate Professor
Electronics and Communication Engineering Dept.,
National Institute of Technology Durgapur
Durgapur West Bengal*

Prof. Fong-Gong Wu

*College of Planning and Design, National Cheng Kung
University
Taiwan*

Dr. Abha Mishra.

*Senior Research Specialist & Affiliated Faculty.
Thailand*

Dr. Madad Khan

*Head
Department of Mathematics
COMSATS University of Science and Technology
Abbottabad, Pakistan*

Prof. Yuan-Shyi Peter Chiu

*Department of Industrial Engineering & Management
Chaoyang University of Technology
Taichung, Taiwan*

Dr. M. R. Pahlavani,

*Head, Department of Nuclear physics,
Mazandaran University,
Babolsar-Iran*

Dr. Subir Das,

*Department of Applied Mathematics,
Institute of Technology, Banaras Hindu University,
Varanasi*

Dr. Anna Oleksy

*Department of Chemistry
University of Gothenburg
Gothenburg,
Sweden*

Prof. Gin-Rong Liu,

*Center for Space and Remote Sensing Research
National Central University, Chung-Li,
Taiwan 32001*

Prof. Mohammed H. T. Qari

*Department of Structural geology and remote sensing
Faculty of Earth Sciences
King Abdulaziz UniversityJeddah,
Saudi Arabia*

Dr. Jyhwen Wang,

*Department of Engineering Technology and Industrial
Distribution
Department of Mechanical Engineering
Texas A&M University
College Station,*

Prof. N. V. Sastry

*Department of Chemistry
Sardar Patel University
Vallabh Vidyanagar
Gujarat, India*

Dr. Edilson Fereda

*Graduate Program on Knowledge Management and IT,
Catholic University of Brasilia,
Brazil*

Dr. F. H. Chang

*Department of Leisure, Recreation and Tourism
Management,
Tzu Hui Institute of Technology, Pingtung 926,
Taiwan (R.O.C.)*

Prof. Annapurna P.Patil,

*Department of Computer Science and Engineering,
M.S. Ramaiah Institute of Technology, Bangalore-54,
India.*

Dr. Ricardo Martinho

*Department of Informatics Engineering, School of
Technology and Management, Polytechnic Institute of
Leiria, Rua General Norton de Matos, Apartado 4133, 2411-
901 Leiria,
Portugal.*

Dr Driss Miloud

*University of mascara / Algeria
Laboratory of Sciences and Technology of Water
Faculty of Sciences and the Technology
Department of Science and Technology
Algeria*

Prof. Bidyut Saha,

*Chemistry Department, Burdwan University, WB,
India*

ARTICLES

Slip flow of a second grade fluid past a lubricated rotating disc 96

K. Mahmood, M. Sajid, N. Ali and T. Javed

Purity-performance relationship of anthocyanidins as sensitizer in dye-sensitized solar cells 104

Ibrahim Olasegun A., Bello Isah A., Semire Banjo, Bolarinwa Hakeem S. and Boyo Adenike

Full Length Research Paper

Slip flow of a second grade fluid past a lubricated rotating disc

K. Mahmood*, M. Sajid, N. Ali and T. Javed

Department of Mathematics and Statistics, International Islamic University, Islamabad 44000, Pakistan.

Received 1 January, 2016; Accepted 31 March, 2016

Slip flow of a second-grade fluid past a lubricated rotating disc is studied. The disc is lubricated with a power-law fluid. The interfacial conditions between fluid and lubricant are imposed on the surface of disc by assuming a thin lubrication layer. The numerical solutions are obtained using Keller-Box method. The effects of slip parameter and Weissenberg number on the three components of fluid velocity and pressure are analyzed graphically while effects on both components of skin friction are demonstrated through tables. The computed results show that spin-up by a second grade bulk fluid near the rotating disc is reduced by increasing slip at the interface. The obtained solutions agree well in the special case with those of other researches.

Key words: Non-Newtonian power-law fluid, second grade fluid, rotating disc, slip boundary condition.

INTRODUCTION

Technical applications of the flow over a rotating surface occur in many engineering and industrial fields. Some direct applications of flow over a rotating disc are waste water treatment, turbo-machinery, viscometry, centrifugal pumps, computer discs, sports discs, and rotating blades. The stagnation point flow of Newtonian fluid over a rotating disc was initially discussed by Von Karman (1921), who transformed the set of partial differential equations into ordinary differential equations by introducing an elegant similarity transformation and solved the resulting equations by momentum integral method. Due to the importance of rotating flows in the fields of engineering and technology, much extensions and modifications with more accurate solutions of Von

Karman's flow have been presented in the literature. Cochran (1934) obtained asymptotic solution of the Von Karman's flow problem. Benton (1966) improved the Cochran's results and extended the problem by taking into account the unsteady case. Sparrow and Gregg (1960) studied the steady state heat transfer from a rotating disc by taking different values of Prandtl numbers. Kakutani (1962), Sparrow and Chess (1962), Pande (1971), Watson and Wang (1979), Kumar et al. (1988) and Watanabe and Oyama (1991) discussed different aspects of electrically conducting viscous fluid over a rotating disc with heat transfer. Turkyilmazoglu (2015) analyzed Bödewadt flow and heat transfer over a stretching disk. Asghar et al. (2014) carried out Lie group

*Corresponding author. E-mail: khalidmeh2012@gmail.com.

analysis of flow and heat transfer of a viscous fluid on a rotating disk stretching in radial direction. In recent years, Turkyilmazoglu (2014); Turkyilmazoglu and Senel, (2013); Turkyilmazoglu, (2012a; b); Turkyilmazoglu, (2009) investigated different aspects of fluid flow and heat transfer due to rotating disc. Effects of slip at permeable disc are investigated by Miklavcic and Wang (2004). Hannah (1947) discussed the axisymmetric stagnation point flow of a viscous fluid towards a rotating disc for the first time. Tifford and Chu (1952) found the exact solution of the problem considered by Hannah (1947). Wang (2008) studied stagnation-point flow over an off-centered rotating disc and proved that non alignment complicates the flow problem. Asghar et al. (2007) investigated MHD flow due to non-coaxial rotation of an accelerated disc. Attia (2009) studied the flow due to a rotating disc under the influence of an external uniform magnetic field. In 2003, Wang (2003) investigated the stagnation point flow for a flat plate in the presence of slip boundary condition. The slip flow over a lubricated rotating disc was first considered by Andersson and Rousselet (2006). The axisymmetric stagnation point flow of a viscous fluid on a surface lubricated with a power-law fluid has been carried out by Santra et al. (2007).

In all the aforementioned studies, constitutive relationship of a viscous fluid is considered. However, fluids used in industry and technology do not obey Newton's law of viscosity and are called non-Newtonian fluids. For example, polymer solutions and melts, oil, paints, blood, etc., for which Navier-Stokes equations are inadequate. A number of non-Newtonian models have been proposed to predict the phenomena like normal stress effects, shear thinning, shear thickening, stress relaxation and retardation, etc. Amongst these non-Newtonian fluids, the second grade fluid is one that has been studied extensively. The equation of motion for second grade fluid is highly non-linear and one order higher than the Navier-Stokes equations. Therefore, to obtain a well posed problem, one requires additional boundary conditions to study the flow problems. Rajagopal and Gupta (1984) showed that to obtain a unique solution for the flow of a second-grade fluid in bounded geometry, an additional boundary condition is required. To overcome the requirement of additional boundary conditions, Beard and Walters (1964) discussed the stagnation point flow of a viscoelastic fluid by using a regular perturbation technique in which the perturbation parameter is the coefficient of the highest derivative. Garg and Rajagopal (1990) and Ariel (2002) augmented the boundary conditions at infinity in order to overcome this difficulty. In another investigation, Ariel (1997) studied the steady laminar flow of a second grade fluid near a rotating disc. Labropulu and Li (2008) discussed stagnation point flow of a second grade fluid with slip. MHD mixed convection in a vertical annulus filled with Al_2O_3 -water nano-fluid considering nanoparticles

migration was analyzed by Malvandi et al. (2015). Recently Afrand et al. (2015) discussed effects of magnetic field on free convection flow in inclined cylindrical annulus containing molten Potassium. Safaei et al. (2011) investigated numerical study of laminar mixed convection heat transfer of power-law non-Newtonian fluids in square enclosures by Finite Volume Method. A literature survey reveals that there is no attempt available for studying the slip flow of a second grade fluid over a lubricated rotating disc. The slip boundary condition at the interface between the second grade and power-law fluids is developed and numerical results are computed to discuss the behaviour of second grade fluid over a lubricated disk. The obtained results for a second grade fluid show a significant deviation from the available results for Newtonian fluid. The results for no-slip case are deduced as the special case from the obtained solutions. An implicit finite difference scheme known as Keller-Box method (Keller and Cebeci, 1972; Bradshaw et al., 1981; Keller, 1970) is employed to obtain the similarity solution.

MATHEMATICAL FORMULATION

Consider the steady, axisymmetric flow of a second grade fluid over a rotating disc lubricated with a thin layer of power law fluid. The flow rate Q of the lubricant is given by

$$Q = \int_0^{\delta(r)} U(r, z) 2\pi r dz, \quad (1)$$

where $U(r, z)$ is the radial component of the velocity vector of power-law fluid and $\delta(r)$ is the variable thickness of the lubrication layer. Moreover, disc is rotating with a uniform velocity ω about z -axis which is normal to the disc and the origin O is located at the center of the disc (Figure 1).

In the presence of these assumptions, the flow of a second grade fluid is governed by the following equations:

$$\nabla \cdot \mathbf{v} = 0, \quad (2)$$

$$\rho(\mathbf{v} \cdot \nabla \mathbf{v}) = -\nabla P + \mu \nabla^2 \mathbf{v} - k_0 \{\nabla^2(\mathbf{v} \cdot \nabla) \mathbf{v} - 2(\mathbf{v} \cdot \nabla) \nabla^2 \mathbf{v}\}, \quad (3)$$

where $P(r, z)$ is the fluid pressure, ρ is density, μ is viscosity and k_0 is the second grade fluid parameter. The boundary condition at the surface is

$$U(r, 0) = 0, V(r, 0) = \omega r, W(r, 0) = 0, P(r, 0) = 0. \quad (4)$$

with

$$W(r, z) = 0, \quad \forall z \in [0, \delta(r)]. \quad (5)$$

The continuity of the shear stress at the interface $z = \delta(r)$ for both the fluids suggests:

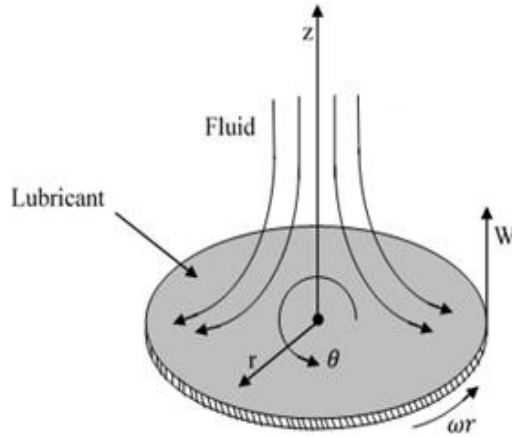


Figure 1. Diagram showing considered flow problem.

$$\mu \left(\frac{\partial u}{\partial z} \right) + k_0 \left(-\frac{v}{r} \frac{\partial v}{\partial z} - \frac{\partial u}{\partial z} \frac{\partial w}{\partial z} + \frac{\partial u}{\partial z} \frac{\partial u}{\partial r} + \frac{\partial v}{\partial z} \frac{\partial v}{\partial r} + \frac{\partial w}{\partial z} \frac{\partial w}{\partial r} - \frac{\partial u}{\partial r} \frac{\partial w}{\partial z} + u \frac{\partial^2 u}{\partial r \partial z} + w \frac{\partial^2 u}{\partial z^2} + w \frac{\partial^2 w}{\partial r \partial z} + u \frac{\partial^2 w}{\partial r^2} \right) = \mu_L \frac{\partial u}{\partial z}, \quad (6)$$

$$\mu \left(\frac{\partial v}{\partial z} \right) + k_0 \left(\frac{u}{r} \frac{\partial v}{\partial z} - \frac{\partial v}{\partial z} \frac{\partial w}{\partial z} + w \frac{\partial^2 v}{\partial z^2} + \frac{v}{r} \frac{\partial w}{\partial r} - \frac{\partial v}{\partial r} \frac{\partial w}{\partial z} + u \frac{\partial^2 v}{\partial r \partial z} \right) = \mu_L \frac{\partial v}{\partial z}. \quad (7)$$

In Equations 6 and 7, μ_L is the viscosity of the power law fluid. Assuming

$$\frac{\partial U}{\partial r} \ll \frac{\partial U}{\partial z} \text{ and } \frac{\partial V}{\partial r} \ll \frac{\partial V}{\partial z}, \mu_L \text{ can be written as}$$

$$\mu_L = k \left[\left(\frac{\partial U}{\partial z} \right)^2 + \left(\frac{\partial V}{\partial z} \right)^2 \right]^{\frac{n-1}{2}}, \quad (8)$$

where k is the consistency coefficient and n is the flow behavior index of the power-law fluid. Assuming the linear variations of the radial and circumferential velocity components of power-law fluid inside the lubrication layer, we get

$$U(r, z) = \frac{\tilde{U}(r)z}{\delta(r)}, \quad (9)$$

$$V(r, z) = \omega r - \frac{(\omega r - \tilde{V}(r))z}{\delta(r)}. \quad (10)$$

Here $\tilde{U}(r)$ and $\tilde{V}(r)$ are interfacial velocity components of bulk second grade fluid and power law fluid. Thickness of the lubrication layer can be evaluated by substituting Equation 9 into Equation 1:

$$\delta(r) = \frac{Q}{\pi r \tilde{U}(r)}. \quad (11)$$

Since at the interface

$$\tilde{U} = u, \tilde{V} = v \quad (12)$$

Therefore, Equations 6 and 7 yield

$$\frac{\partial u}{\partial z} + \frac{k_0}{\mu} \left(-\frac{v}{r} \frac{\partial v}{\partial z} - \frac{\partial u}{\partial z} \frac{\partial w}{\partial z} + \frac{\partial u}{\partial z} \frac{\partial u}{\partial r} + \frac{\partial v}{\partial z} \frac{\partial v}{\partial r} + \frac{\partial w}{\partial z} \frac{\partial w}{\partial r} - \frac{\partial u}{\partial r} \frac{\partial w}{\partial z} + u \frac{\partial^2 u}{\partial r \partial z} + w \frac{\partial^2 u}{\partial z^2} + w \frac{\partial^2 w}{\partial r \partial z} + u \frac{\partial^2 w}{\partial r^2} \right) = \frac{k}{\mu} \left(\frac{\pi}{Q} \right)^n u (ru)^n [u^2 + (\omega r - v)^2]^{\frac{n-1}{2}}, \quad (13)$$

$$\frac{\partial v}{\partial z} + \frac{k_0}{\mu} \left(\frac{u}{r} \frac{\partial v}{\partial z} - \frac{\partial v}{\partial z} \frac{\partial w}{\partial z} + w \frac{\partial^2 v}{\partial z^2} + \frac{v}{r} \frac{\partial w}{\partial r} - \frac{\partial v}{\partial r} \frac{\partial w}{\partial z} + u \frac{\partial^2 v}{\partial r \partial z} \right) = -\frac{k}{\mu} \left(\frac{\pi}{Q} \right)^n (\omega r - v) (ru)^n [u^2 + (\omega r - v)^2]^{\frac{n-1}{2}}. \quad (14)$$

Furthermore, the continuity of the axial velocity components at the interface gives

$$w(r, \delta(r)) = W(r, \delta(r)) = 0, \quad (15)$$

Assuming that the lubrication layer is very thin, boundary conditions (13), (14) and (15) can be imposed at the surface when $z = 0$ as proposed by Andersson and Rousselet (2006).

The free stream boundary conditions are given by

$$u = 0, v = 0. \quad (16)$$

To solve the system of partial differential equations obtained from Equation 3, the following dimensionless variables were introduced:

$$\eta = z \sqrt{\frac{\omega}{v}}, u = \omega r f(\eta), v = \omega r g(\eta), w = \sqrt{\omega v} h(\eta), P = \omega \mu p(\eta) \quad (17)$$

The reduced system of coupled non-linear ordinary differential equations along with boundary conditions is

$$h' = -2f \quad (18)$$

$$f'' - hf' - f^2 + g^2 + We(hf'''' + 4ff'' + 2g'^2) = 0, \quad (19)$$

$$g'' - hg' - 2fg + We(hg'''' + 4fg'' - 2f'g') = 0, \quad (20)$$

$$p' + 2f' - 2fh + We(12ff' + 2f''h) = 0. \quad (21)$$

$$h(0) = 0, p(0) = 0, \quad (22)$$

$$f'(0) + We[2f(0)f'(0) - f'(0)h'(0) + h(0)f''(0)] = \lambda(f(0))^{\frac{1}{2}}[(f(0))^2 + (1-g(0))^2]^{-1/3} \quad (23)$$

$$g'(0) + We[2f(0)g'(0) - g'(0)h'(0) + h(0)g''(0)] = -\lambda(f(0))^{\frac{1}{2}}(1-g(0))[(f(0))^2 + (1-g(0))^2]^{-1/3} \quad (24)$$

$$f(\infty) = 0, g(\infty) = 0 \quad (25)$$

where $We = k_0 \omega / \rho v$ is the Weissenberg number and

$$\lambda = \frac{k\sqrt{v}}{\mu} \left(\frac{\pi}{Q} \right)^{\frac{1}{3}} \frac{\omega^{\frac{2}{3}}}{\omega^{\frac{2}{3}}}. \quad (26)$$

It is worth mentioning that we have used $n = 1/3$ in Equations 23 and 24 in order to obtain similarity solution. From Equation 26, the constant λ can be written as

$$\lambda = \frac{\sqrt{\frac{\nu}{\omega}}}{\frac{\mu(Q\omega)^{\frac{1}{3}}}{k(\frac{\pi}{\pi})^{\frac{1}{3}}}} = \frac{L_{visc}}{L_{lub}} \quad (27)$$

It is clear from Equation 27 that the parameter λ is the ratio of viscous length and lubrication length scales, respectively. When the lubricant is highly viscous and the lubrication length is small, λ becomes large. In the limiting case when $\lambda \rightarrow \infty$, the conventional no-slip conditions $f(0) = 0$ and $g(0) = 1$ are obtained from Equations 23 and 24. In the reverse case, when $\lambda \rightarrow 0$, one obtains the full-slip boundary conditions $f'(0) = 0$ and $g'(0) = 0$. Hence, λ is known as slip parameter.

NUMERICAL RESULTS AND DISCUSSION

To analyze the behaviour of parameters λ and We on velocity and pressure profiles, the Equations 18 to 21 together with boundary conditions 22 to 25 are solved numerically by the Keller-Box method (Keller and Cebeci, 1972; Bradshaw et al., 1981; Keller, 1970).

Figures 2 to 6 are plotted to see the effects of slip parameter λ on velocity profiles f , g , h and pressure p for some fixed values of Weissenberg number, while the effects of We in the presence of slip are shown in Figures 6 to 10. Dashed lines shown in Figures 2 to 6 are the reproduced results already calculated by Andersson and Rousselet (2006) through Keller-Box method for the case of Newtonian fluid (that is, $We = 0$). Numerical computations for both the components of skin friction coefficients under the influence of pertinent parameters are presented in Tables 1 to 2.

Figure 2 is displayed to show the effects of slip parameter λ on axial velocity when $We = 1$. It is important to mention here that as the numerical values of λ is increased, an increase in the value of $-h$ is observed. Also, the thickness of boundary layer region is increased by increasing the numerical value of λ . Figure 3 shows the variation in the radial velocity f caused by the centrifugal force under the influence of slip parameter. It is clear from Figure 3 that by increasing slip on the surface, f decreases. The variation in radial velocity has the same behaviour as observed for the viscous fluid (dashed lines) except the peak value which was near 0.18 at $\eta = 0.90$ for the viscous fluid when there is no-slip (2006) and is now near 0.225 when η is about 1.1 (near unity) for the second grade fluid. The gradual increase in the radial velocity in Figure 3 with increasing value of λ is directly related with the distributions of the h -profile shown in Figure 2. This is due to the direct relation between f and h shown in Equation 18.

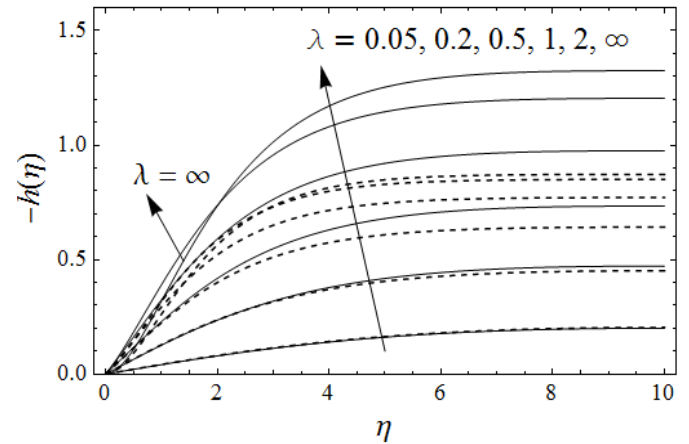


Figure 2. Variation of $-h(\eta)$ for different values of λ when $We = 1$. Dashed lines are calculated by Andersson and Rousselet (2006).

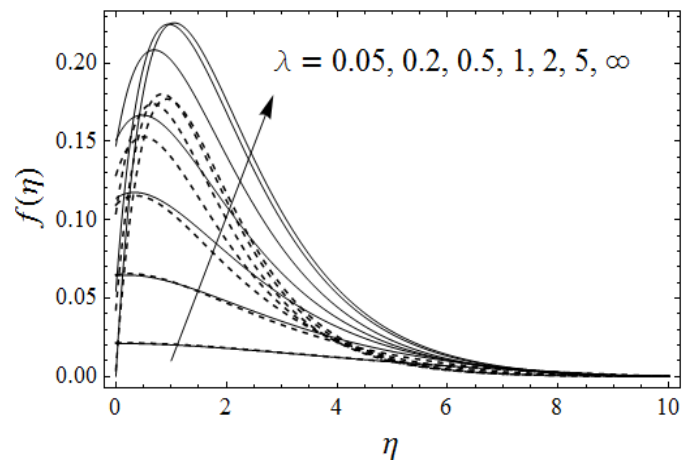


Figure 3. Variation of $f(\eta)$ for different values of λ when $We = 1$. Dashed lines are calculated by Andersson and Rousselet (2006).

Effect of slip parameter on the azimuthal velocity component g in the circumferential direction is depicted in Figure 4. It is obvious from Figure 4 that by increasing λ , the numerical value of g is increased. The torque required to maintain steady rotation of the disc is controlled by this component of the velocity. The imposed torque decreases monotonically by increasing slip on the surface. It is evident from Figures 2 to 4 that the variation in the three velocity components is more significant for smaller values of λ showing that power-law lubricant increases the fluid velocity at the surface.

The variation in the pressure under the influence of slip parameter when $We = 1$, is observed in Figures 5 and 6.

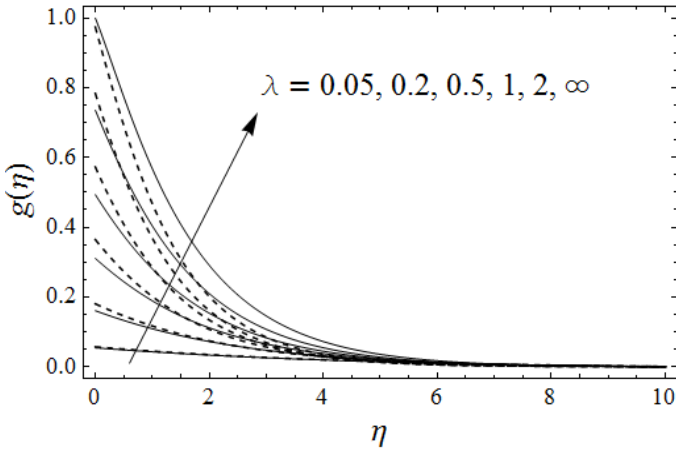


Figure 4. Variation of $g(\eta)$ for different values of λ when $We = 1$. Dashed lines are calculated by Andersson and Rousselet (2006).

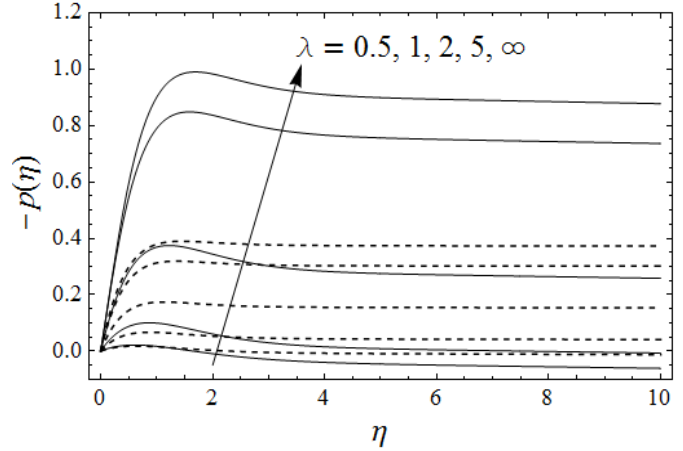


Figure 6. Effect of slip on pressure when $We = 1$.

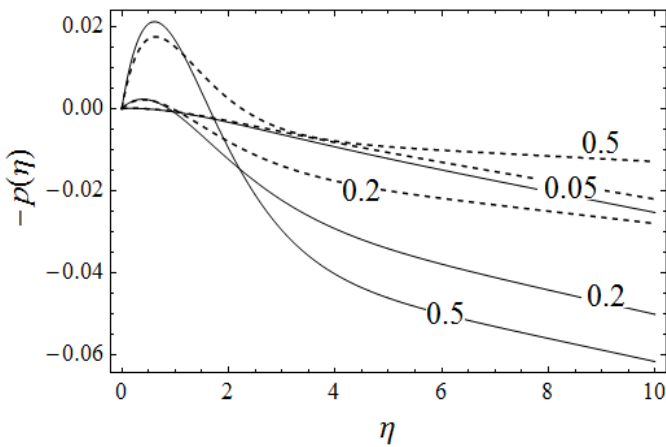


Figure 5. Effect of slip on pressure when $We = 1$.

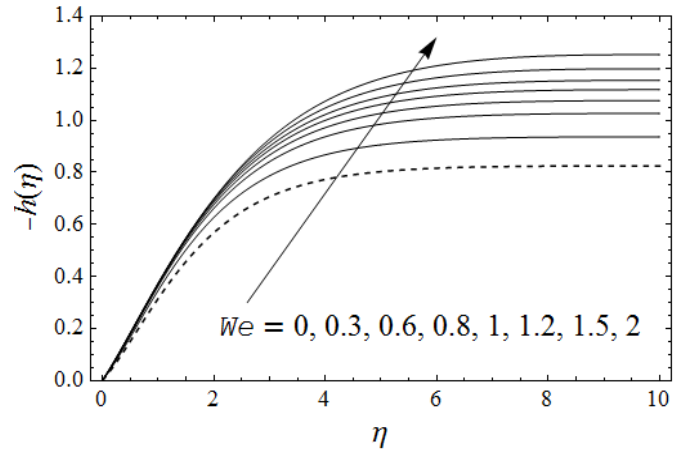


Figure 7. Variation of $-h(\eta)$ for different values of We when $\lambda = 1.5$.

It is clear from Figure 6 that pressure increases by decreasing slip. However, the behaviour of pressure distribution near the full slip is different as shown in the Figure 5. For $\lambda \leq 1$ the disc pressure is less than the ambient pressure $-p(\infty)$, which means that the flow is driven towards the disc by the axial pressure gradient in this particular range of λ .

Effect of We on h -profile when $\lambda = 1.5$ is shown in Figure 7. It is obvious from this figure that by increasing We , the axial velocity component is increased. The velocity profile shown by dashed line is for viscous fluid, that is, when $We = 0$. Figure 8 shows the variation in radial velocity component f when We ranges from 0 to 5 and $\lambda = 1.5$. It is evident from this figure that f

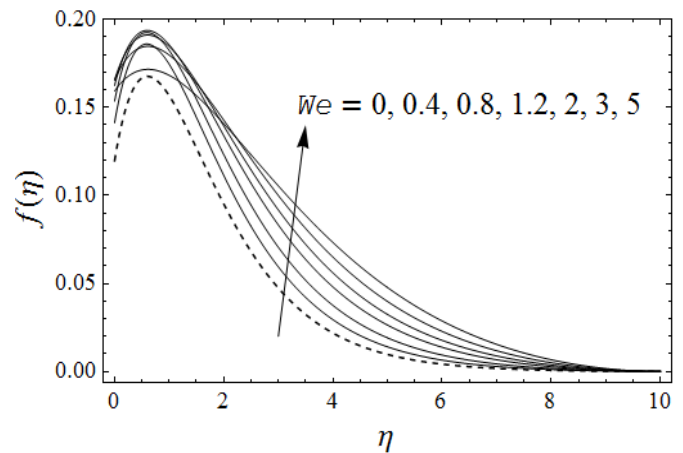


Figure 8. Variation of $f(\eta)$ for different values of We when $\lambda = 1.5$.

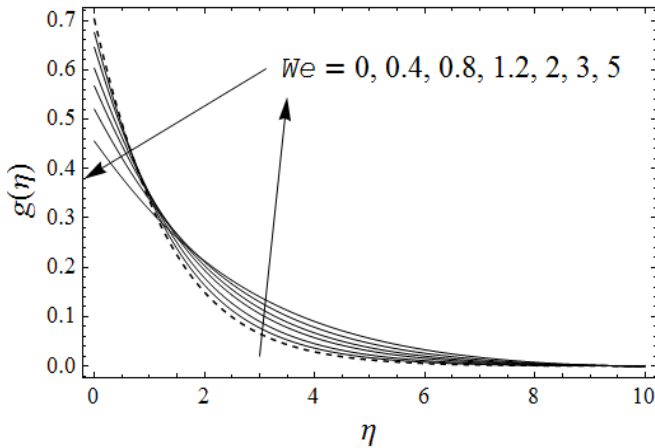


Figure 9. Variation of $g(\eta)$ for different values of We when $\lambda = 1.5$.

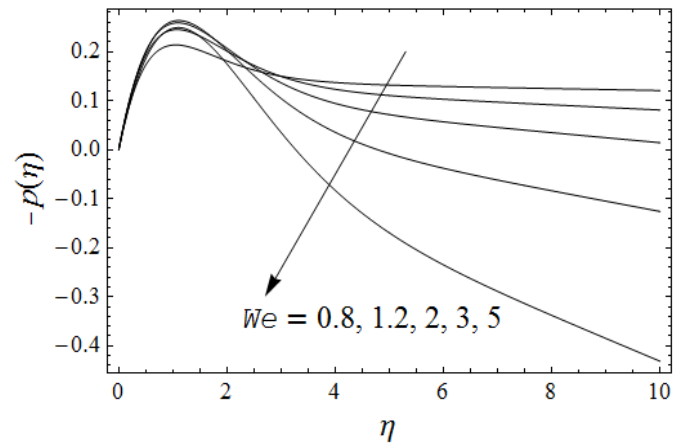


Figure 11. Variation of $-p(\eta)$ for different values of We when $\lambda = 1.5$.

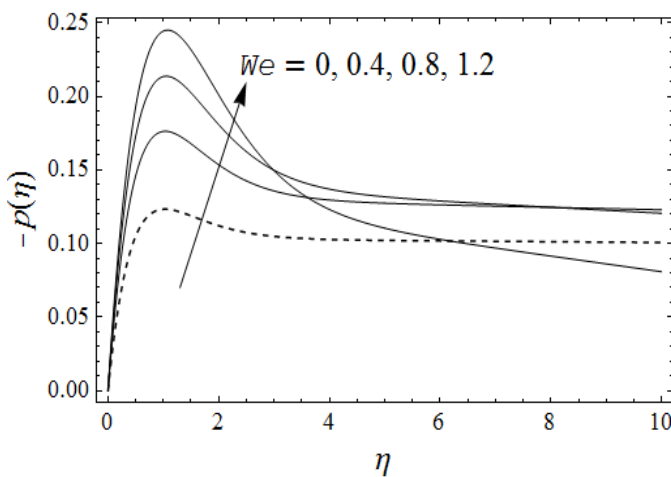


Figure 10. Variation of $-p(\eta)$ for different values of We when $\lambda = 1.5$.

increases with an increase in Weissenberg number. Some reverse effects was observed on the peak for higher values of We . The azimuthal velocity component g is presented in Figure 9. It is evident from this figure that g increases by increasing the value of We when λ is fixed. An opposite behaviour in the shear component of velocity is observed near the surface. Figures 10 and 11 are plotted for the pressure distribution using various values of We when $\lambda = 1.5$. It is clear from these figures that $-p$ increases when $0 \leq We < 0.8$. After this pressure profile shows an increase near the surface and then decreases dramatically.

Table 1 elucidates the change in numerical values of $f'(0)$ and $g'(0)$ for various values of λ when $We = 0.05$ and $We = 1$. It is clear from the Table 1 that as λ increases from 0 to ∞ , the numerical values of $f'(0)$ increase. However, the numerical values of $g'(0)$ initially increase and then start decreasing. The numerical values of $f'(0)$ and $g'(0)$ for different values of We when $\lambda = 0.05$ and $\lambda = 1.5$ are presented in Table 2. According to this table as the numerical value of We increases, the numerical values of $f'(0)$ increase while those of $g'(0)$ decrease.

Conclusion

In this paper, the slip flow of a second grade fluid over a rotating disc lubricated with a thin layer of power-law fluid was examined. The governing equations along with boundary conditions are transformed to ordinary differential equations by a suitable choice of transformation. To obtain true similarity solutions, we selected $n = 1/3$. The numerical solutions were computed using Keller-Box method. The motivation is to determine the effects of the slip parameter λ and We on the flow characteristics. The cases of full slip for $\lambda \rightarrow 0$ and no slip for $\lambda \rightarrow \infty$ can be deduced from the present results. The main findings are investigated as under.

As the slip increases the numerical values of all the three components of velocity are decreased. Numerical value of all velocity components is decreased as We is decreased.

An unexpected reversal in the pressure gradient has been observed for the lower values of λ and We .

Table 1. Numerical values of $f'(0)$ and $g'(0)$ for various values of λ .

$W_e = 0.05$			$W_e = 1$		
λ	$f'(0)$	$g'(0)$	λ	$f'(0)$	$g'(0)$
0.01	-0.000119	0.000056	0.01	-0.000119	0.000055
0.05	-0.002743	0.002407	0.05	-0.002556	0.002074
0.1	-0.008848	0.007804	0.1	-0.007839	0.006160
0.5	-0.119575	0.077270	0.5	-0.086636	0.043736
1.0	-0.311114	0.141201	1.0	-0.220373	0.068210
2.0	-0.614639	0.152593	2.0	-0.518510	0.029763
5.0	-0.908031	0.056128	5.0	-1.053342	-0.261694
10	-0.990542	0.004268	10	-1.232311	-0.406746
50	-1.032491	-0.028260	50	-1.320843	-0.484123
100	-1.035151	-0.030489	100	-1.326394	-0.489068
500	-1.036475	-0.031607	500	-1.329053	-0.491426
∞	-1.036605	-0.031717	∞	-1.329155	-0.491531

Table 2. Numerical values of $f'(0)$ and $g'(0)$ for various values of We .

$\lambda = 0.05$			$\lambda = 1.5$		
We	$f'(0)$	$g'(0)$	We	$f'(0)$	$g'(0)$
0	-0.002753	0.002427	0	-0.478938	0.168179
0.001	-0.002753	0.002427	0.001	-0.479043	0.168021
0.01	-0.002751	0.002423	0.005	-0.479498	0.167321
0.05	-0.002743	0.002407	0.01	-0.480046	0.166445
0.1	-0.002733	0.002388	0.05	-0.483640	0.159458
0.6	-0.002635	0.002206	0.1	-0.486222	0.150860
1.0	-0.002556	0.002074	0.5	-0.453483	0.096387
1.5	-0.002461	0.001925	1	-0.368705	0.062445
2	-0.002370	0.001791	1.5	-0.294832	0.046572
3	-0.002202	0.001565	2	-0.239556	0.037693
5	-0.001922	0.001230	3	-0.168367	0.027724
10	-0.001462	0.000766	5	-0.100475	0.018027

The computed results show that spin-up by second grade bulk fluid near the rotating disc is reduced by increasing slip. The radially directed centrifugal force is also reduced. The radial slip is turned out to be insufficient to outweigh the reduced centrifugal force.

The numerical values of $f'(0)$ increase as λ increases from 0 to ∞ . However, the numerical values of $g'(0)$ initially increase and then start decreasing.

As Weissenberg number We increase, the numerical values of $f'(0)$ increase while those of $g'(0)$ decrease.

Conflict of Interests

The authors have not declared any conflict of interests.

Nomenclature

- Q : Flow rate
 P : Fluid pressure
 δ : Thickness of lubrication layer
 r, θ, z : Cylindrical coordinates
 u, v, w : Velocity components of second grade fluid in radial, azimuthal and axial direction
 ρ : Density
 μ : Viscosity of second grade fluid
 k_0 : Material parameter
 ω : Velocity of disc
 λ : Slip parameter
 μ_L : Viscosity of power-law fluid
 U, V, W : Velocity components of Power-law fluid in radial, azimuthal and axial direction
 n : Flow behavior index of Power-law fluid
 We : Weissenberg number
 k : Consistency coefficient of power-law fluid.

REFERENCES

- Afrand M, Sina N, Teimouri H, Mazaheri A, Safaei MR, Esfe MH, Kamali J, Toghraie D (2015). Effect of Magnetic Field on Free Convection in Inclined Cylindrical Annulus Containing Molten Potassium. *Int. J. Appl. Mech.* 7(4):1550052.
- Andersson HI, Rousselet M (2006). Slip flow over a lubricated rotating disc. *Int. J. Heat Fluid Flow* 27:329-335.
- Ariel PD (1997). Computation of flow of a second grade fluid near a rotating disk. *Int. J. Eng. Sci.* 23:1335-1357.
- Ariel PD (2002). On extra boundary condition in the stagnation point flow of a second grade fluid. *Int. J. Eng. Sci.* 40:145-162.
- Asghar S, Hanif K, Hayat T, Khaliq CM (2007). MHD non Newtonian flow due to non-coaxial rotations of an accelerated disk and a fluid at infinity. *Commun. Nonlinear Sci. Num. Simulation* 12:465-485.
- Asghar S, Jalil M, Hussan M, Turkyilmazoglu M (2014). Lie group analysis of flow and heat transfer over a stretching rotating disk. *Int. J. Heat Mass Transfer* 69:140-146.
- Attia HA (2009). Steady flow over a rotating disk in a porous medium with heat transfer. *Nonlinear Anal. Model. Control* 14:21-26.
- Beard BW, Walters K (1964). Elastico-viscous boundary layer flows. I. Two-dimensional flow near a stagnation point. *Proc. Cambridge Philosophical Soc.* 60:667-674.
- Benton ER (1966). On the flow due to a rotating disk. *J. Fluid Mech.* 24:781-800.
- Bradshaw V, Cebeci T, Whitelaw IH (1981). *Engineering Calculation Methods for Turbulent Flows*. Academic, London.
- Cochran WG (1934). The flow due to a rotating disc. *Proc. Cambridge Philosophical Soc.* 30:365-375.
- Garg VK, Rajagopal KR (1990). Stagnation point flow of a non-Newtonian fluid. *Mech. Res. Commun.* 17:415-421.
- Hanna DM (1947). Forced flow against a rotating disc. *British Aeronautical Research Council Reports and Memoranda, No. 2772*, University of Michigan.
- Kakutani T (1962). Hydromagnetic flow due to a rotating disk. *J. Phys. Soc. Japan* 17:1496-1506.
- Keller HB (1970). A New Difference Scheme for Parabolic Problems, in *Numerical Solution of Partial Differential Equations* (J. Bramble, ed.). Volume II, Academic, New York.
- Keller HB, Cebeci T (1972). *Accurate Numerical Methods for Boundary Layer Flows II: Two Dimensional Turbulent Flows*. Am. Inst. Aeronautics Astronautics 10:1193-1199.
- Kumar SK, Thacker WI, Watson LT (1988). Magnetohydrodynamic flow past a porous rotating disk in a circular magnetic field. *Int. J. Num. Methods Fluids* 8:659-669.
- Labropulu F, Li D (2008). Stagnation-point flow of a second grade fluid with slip. *Int. J. Non-Linear Mech.* 43:941-947.
- Malvandi A, Safaei MR, Kaffash MH, Ganji DD (2015). MHD mixed convection in a vertical annulus filled with Al₂O₃-water nanofluid considering nanoparticle migration. *J. Magnetism Magnetic Mater.* 382:296-3069.
- Miklavcic M, Wang CY (2004). The flow due to a rotating disk. *J. Appl. Math. Phys.* 54:1-12.
- Pande GS (1971). On the effects of uniform high suction on the steady hydromagnetic flow due to a rotating disk. *Appl. Sci. Res.* 11:205-212.
- Rajagopal KR, Gupta AS (1984). An exact solution for the flow of a non-Newtonian fluid past an infinite plate. *Meccanica* 19:158.
- Safaei MR, Rahmian B, Goodarzi M (2011). Numerical Study of Laminar Mixed Convection Heat Transfer of Power-Law Non-Newtonian Fluids in Square Enclosures by Finite Volume Method. *Int. J. Phys. Sci.* 6(33):7456-7470.
- Santra B, Dandapat BS, Andersson HI (2007). Axisymmetric stagnation-point flow over a lubricated surface. *Acta Mechanica* 194:1-10.
- Sparrow EM, Chess RD (1962). Magnetohydrodynamic flow and heat transfer about a rotating disk. *ASME J. Appl. Mechanics* 29:181-187.
- Sparrow EM, Gregg JL (1960). Mass transfer, flow, and heat transfer about a rotating disk. *ASME J. Heat Transfer* 82:294-302.
- Tifford AN, Chu ST (1952). On the flow around a rotating disc in a uniform stream. *J. Aeronautical Sci.* 19:284-285.
- Turkyilmazoglu M (2009). Exact solutions for the incompressible viscous fluid of a porous rotating disk flow. *Int. J. Non-Linear Mechanics* 44(4):352-357.
- Turkyilmazoglu M (2012a). An implicit spectral method for the numerical solution of unsteady flows with an application to rotating disk flow and heat transfer. *Isi Bilimi Ve Teknigi Dergisi*. *J. Thermal Sci. Technol.* 32(2):99-106.
- Turkyilmazoglu M (2012b). Three dimensional MHD stagnation flow due to a stretchable rotating disk. *Int. J. Heat Mass Transfer* 55(23-24):6959-6965.
- Turkyilmazoglu M (2014). MHD fluid flow and heat transfer due to a shrinking rotating disk. *Comput. Fluids* 90:51-56.
- Turkyilmazoglu M (2015). Bödewadt flow and heat transfer over a stretching stationary disk. *Int. J. Mech. Sci.* 90:246-250.
- Turkyilmazoglu M, Senel P (2013). Heat and mass transfer of the flow due to a rotating rough and porous disk. *Int. J. Thermal Sci.* 63:146-158.
- Von KT (1921). Überlaminare und turbulente Reibung. *J. Appl. Math. Mech.* 1:233-252.
- Wang CY (2003). Stagnation flows with slip: Exact solution of the Navier-Stokes equations. *Zeitschrift für Angewandte Mathematik und Phys.* 54:184-189.
- Wang CY (2008). Off-centered stagnation flow towards a rotating disc. *Int. J. Eng. Sci.* 46:391-396.
- Watanabe T, Oyama T (1991). Magnetohydrodynamic boundary layer flow over a rotating disk. *Zeitschrift für Angewandte Mathematik und Mechanik* 71:522-524.
- Watson LT, Wang CY (1979). Deceleration of a rotating disk in a viscous fluid. *Phys. Fluids* 22:2267-2269.

Full Length Research Paper

Purity-performance relationship of anthocyanidins as sensitizer in dye-sensitized solar cells

Ibrahim Olasegun A.^{1*}, Bello Isah A.², Semire Banjo², Bolarinwa Hakeem S.³ and Boyo Adenike⁴

¹Department of Chemical Sciences, Fountain University, Osogbo Nigeria.

²Department of Pure and Applied Chemistry, Ladoke Akintola University of Technology, Ogbomoso, Oyo State. Nigeria.

³Department of Physics, Electronics and Earth Sciences, Fountain University, Osogbo Nigeria.

⁴Department of Physics, Lagos State University, Ojo, Lagos Nigeria.

Received 1 February, 2016; Accepted 31 March, 2016

A comparative analysis between crude and purified extracts obtained from withered leaves of *Terminalia catappa* (*T. catappa*) and pure compounds of anthocyanidins as organic sensitizers in solar cells. The chemical and electronic properties of the extracts and the pure anthocyanidins were examined using spectroscopic studies: ultraviolet (UV), Fourier transform infrared (FT-IR) and gas chromatography coupled with flame ionization detector (GC-FID). Solar cells were fabricated using TiO₂ mesoporous film and the extracts and pure compounds as sensitizers. The prominent transitions in U-V spectra were $n \rightarrow \pi^*$ and $\pi \rightarrow \pi^*$ in nature. There were observed shifts in the wavelengths of the absorptions (around 350 to 380 nm) and a characteristic decrease in the absorption between the crude (TCE) and purified (TCP) extracts. The FT-IR spectra of the crude and purified sample have similar absorbances with bathochromic (red) shifts on the hydroxyl group and hypsochromic (blue) shifts on the benzene ring. The GC-FID chromatograms and spectra revealed the presence of six anthocyanidins and their amounts in mg per 100 g of the sample. The results showed that delphinidin was most abundant, and its quantity increases with purification of the extracts, while other anthocyanidins decreased with purification in both extracts. The photovoltaic performances also increase with purity. The best results were obtained with cyanidin-TiO₂ solar cells with efficiencies up to 2.27%.

Key words: *Terminalia catappa*, anthocyanins, solar cell, efficiency, purification, extracts.

INTRODUCTION

Anthocyanins are water-soluble glycosides of polyhydroxyl and polymethoxyl derivatives of 2-phenylbenzopyrylium or flavylum salts and an anthocyanin without sugar moiety is referred to as an anthocyanidin (Middleton, 2000). Anthocyanins and anthocyanidins have been widely applied in various fields

*Corresponding author. E-mail: aiboldkip@gmail.com. Tel: +234-8054-284-452.

such as sensitizers in dye-sensitized solar cells (DSSCs). DSSC provides a technically and economically credible alternative concept to present day junction photovoltaic devices (Middleton, 2000; Simmonds, 2003). The redox and optical properties of natural pigments (like anthocyanins) make them well suited for a variety of applications (Taofeek et al., 2011; Fossen et al., 2004; Kim et al., 2003; Harborne and Williams, 2000). Anthocyanins from *Terminalia catappa* (*T. catappa*) have been shown to have high antioxidant activity (Jordheim et al., 2006; Boyo et al., 2013) indicating a relatively low oxidation potential (Adenike et al., 2013; Wang et al., 2010). Many research works have examined the qualitative analyses of anthocyanins in parts of plants: leaves, flowers, seeds, etc. (Bisquert et al., 2004; Bisquert, et al., 2006). This study explores the application of the extracts (crude and purified) as sensitizers in photovoltaic, DSSCs. The DSSCs light (from the sun) is absorbed by a sensitizer, which is anchored to the surface of a wide band gap oxide semiconductor, like TiO₂. Charge separation takes place at the interface via photo-induced electron injection from the dye into the conduction band of the solid (Grätzel, 2004; Andre and Neyde, 2006; Pooman and Mehra, 2007). Transition metal coordination compounds (ruthenium polypyridyl complexes) have been used as the effective sensitizers, due to their intense charge-transfer absorption in the whole visible range and highly efficient metal-to-ligand charge transfer (Bisquert et al., 2006; Kelly and Meyer, 2001). However, ruthenium polypyridyl complexes have a heavy metal, which is undesirable from point of view of the environment (Chen et al., 2011; Brouillard et al., 2003). Moreover, the process to synthesize the complexes is complicated and costly (Boyo et al., 2012; Hwan et al., 2011). The availability and low cost of the natural dyes made them better candidates to be used for the same purpose with an acceptable efficiency. The ability of these molecules to convert the light into electricity and to induce redox reactions can be very interesting with respect to their implementation in artificial systems (Duthie et al., 2000; Close and Beadle, 2003), but it has also been faced with challenges of low efficiency and stability. Hence, the examination of the relationship between purity and efficiency of the anthocyanidins in the extracts, of the withered leaves of *T. catappa*, being employed as sensitizers in the fabrication of DSSCs.

EXPERIMENTAL

Extraction and purification of anthocyanidins in *T. catappa*

Plant material and sample preparation

Withered leaves of *T. catappa* were obtained within the campus of Fountain University, Osogbo, Nigeria. The samples were air dried under shade for ten days at room temperature. They were pulverized with the aid of liquidizer.

Extraction and purification of the anthocyanidins

The extraction of the pulverized sample was done using a solvent system that comprised of distilled water, methanol and 1 M HNO₃ in ratio 10: 9: 1, respectively. Fifty gram of the pulverized sample was completely submerged in 175 ml of the solvent system and then covered in air tight glass bottle. Extraction was allowed to proceed for 24 h. The extract was decanted and the solvent reduced by evaporation in water bath at 50 ± 5°C to obtain concentrated extract. The concentrated extracts were stored in dark bottles at room temperature. Anthocyanin purification was done using the method of Taofeek et al. (2011). The filtered extract was transferred into a separatory funnel and "washed" three times with equal volumes of ethylacetate to remove flavones. The third volume of the ethylacetate added to the extract were mixed thoroughly in the separatory funnel and left overnight. The ethylacetate-free layer, containing the partially purified anthocyanin, was obtained. Then, equal volumes of the ethylacetate-free extract and that of 0.5% neutral lead acetate (Pb (COO)₂) solution were mixed and kept in the refrigerator at 4°C for 48 h to ensure complete precipitation of anthocyanin. After 48 h, blue supernatant was found and part of it was discarded. The precipitate was re-suspended in the remaining supernatant and transferred into test tubes and was centrifuged at 5,000 rpm for 5 min. Supernatant (blue in color) and dark precipitate (anthocyanin) were obtained, the remaining supernatant was discarded. About 5 ml of 0.5% solution of sulfuric acid was added to the precipitate to remove lead as lead sulfate (PbSO₄), and the precipitate was simultaneously re-solubilized to give a red solution. The mixture was filtered to remove the PbSO₄ and the filtrate. The filtrate was concentrated in a water bath at 50 ± 5°C to obtain the purified anthocyanin, which was stored in a dark plastic bottle in a refrigerator until use.

Structural elucidation of the samples using ultraviolet (UV), Fourier transform infrared (FT-IR) and gas chromatography coupled with flame ionization detector (GC-FID)

Absorption spectroscopy

UV-visible absorbance spectra of TCE and TCP were scanned between 350 and 1,000 nm with a PerkinElmer UV-visible spectrometer (Lambda EZ201; PerkinElmer, Waltham, Massachusetts, USA).

Fourier transform infrared (FT-IR)

The FT-IR was done under high vacuum (10 mbar) conditions using FT-IR over the 4000 to 350 cm⁻¹ spectra range at 500 cm⁻¹ resolution.

Gas chromatography coupled with flame ionization detector (GC-FID)

The type and amount of the anthocyanins in the extracts were determined using GC-FID HP6890 powered with HP chem. Station Rev. A.09.01 (1206) software.

Photovoltaic studies

Preparation and deposition of titanium dioxide (TiO₂) film

TiO₂ film was prepared using the methods of Boyo et al. (2013). Glass plates coated with a conductive layer of fluorine doped SnO₂ (obtained from Hartford Glass Co. Inc., P.O. Box 613, Hartford City,

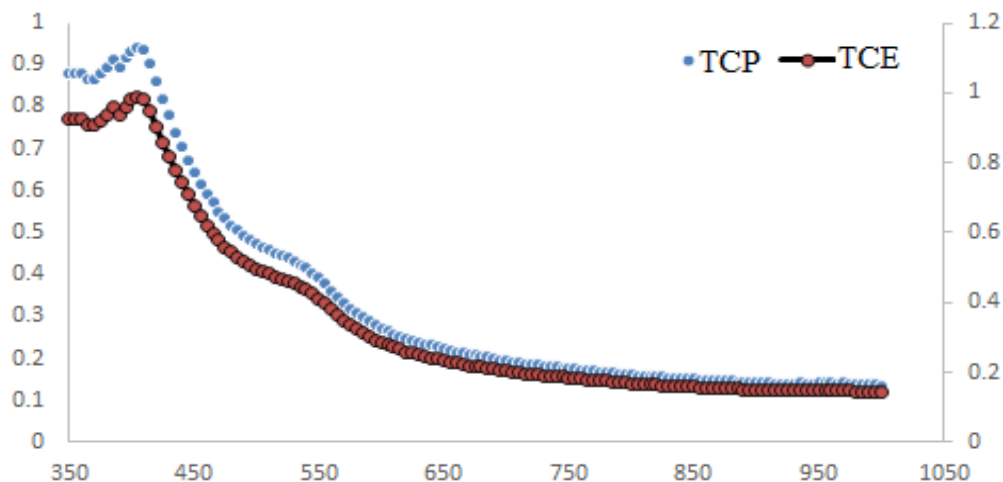


Figure 1. U-V spectra of the crude and purified (TCE and TCP) extracts of *T. catappa* respectively.

IN 47348, USA, Fax 765-348-5435) and the cells were prepared using the methods of Grätzel (2004).

Staining of the titanium dioxide with the dye

Concentrated samples (0.1 g each) were dissolved in 10 ml of distilled deionized water, filtered and used as dye solution (Takeda et al., 1994). TiO₂ coated glass plate was soaked (facing the dye solution) for 10 min in each of the various types of anthocyanin extracts, until the white TiO₂ paste could not be seen upon viewing the stained film from either side of the supporting glass plate.

Carbon coating the counter electrode

While the TiO₂ electrode was being stained in the anthocyanin solution, the counter electrode was made from another piece of conductive SnO₂ coated glass using the method of Grätzel (2004). The carbon-coated counter electrode was annealed at 450°C for about 5 min (Kalaiganan and Kang, 2006). The thin carbon layer served as a catalyst for the tri-iodide to iodide regeneration reaction (Kay and Grätzel, 2002).

Assembling the solar cell and measuring the photovoltaic characteristics

The solar cells were assembled using the methods of Grätzel (2004), Bisquert, et al. (2006) and Boyo et al. (2013). The completed solar cell/light detector was taken for indoor measurements, the cell was illuminated by a 50 W (GE 12V) Tungsten Halogen lamp equipped with integral parabolic reflector and UV and IR blocking filter. The full current-voltage (I-V) curves were measured using a 1000 Ω potentiometer as a variable load. The current density (J_{sc}), open circuit voltage (V_{oc}), fill factor (FF) and the efficiency (η) were used to characterize the performance of the solar cells.

The maximum power density occurs somewhere between $V = 0$ (short circuit) and $V = V_{oc}$ (open circuit) at a voltage V_m . The corresponding current density, J_m and the maximum power density $P_m = J_m V_m$. In these studies, P_s used was 50 W throughout.

RESULTS AND DISCUSSION

In Figure 1, the U-V spectra of the extracts of *T. catappa* are shown. The spectra of the extracts were relatively similar with purified extract having higher absorbance than the crude extract. The implication is that the extracts have similar chemical (or electronic) properties with the crude having compounds that inhibit its electronic properties. In Figure 2, the U-V spectra of the pure anthocyanidins are shown. The spectra of the pure compounds absorbed at close wavelengths in the order Cy> Pg> Dp> Mv. This implied that the compounds have similar functional group(s). In all the samples, the nature of electronic transitions were predominantly $\pi - \pi^*$ and $n - \pi^*$ transitions. The former implied the transitions as results conjugations and aromaticity while the latter are transitions as a result lone pair of electrons.

The FT-IR spectra of the crude and purified extracts have similar absorbances, even at the finger print regions. The spectra of the crude and purified extracts have similar absorbances, ditto for those of pure anthocyanidins, even at the finger print regions. This implied that the extracts have similar functional groups. However, the spectra of the purified samples have bathochromic (red) shifts on the hydroxyl group and hypsochromic (blue) shifts on the benzene ring. The GC-FID chromatograms revealed the presence of six anthocyanidins in the crude and purified extracts, as well as the quantity of the anthocyanidins (Table 1) in mg per 100 g of the sample. The results showed that delphinidin was 86% abundant in TCE and 92.97% in TCP. It was observed that the quantity of the delphinidin increased with purity of the extract, while the amount of others decreased with purity.

The results obtained for the four quantities; current density (J_{sc}), open circuit voltage (V_{oc}), fill factor (FF) and the efficiency (η), are presented as Table 2. In Figure 3,

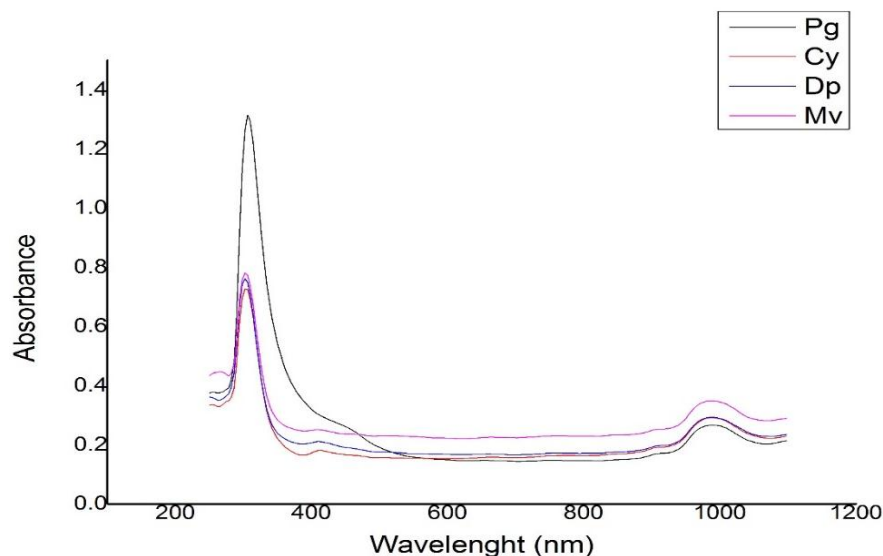


Figure 2. U-V spectra of the pure anthocyanidins.

Table 1. U-V absorbance and peaks of the extracts and pure anthocyanidins.

Sample	Absorbance	Wavelength (nm)	Nature of transition
TCE	3.000	320	$\pi \rightarrow \pi^*$
	1.820	410	$n \rightarrow \pi^*$
TCP	3.000	320	$\pi \rightarrow \pi^*$
Pg	0.417	320	$\pi \rightarrow \pi^*$
Cy	0.108	330	$\pi \rightarrow \pi^*$
Dp	0.109	330	$\pi \rightarrow \pi^*$
Mv	0.115	305	$\pi \rightarrow \pi^*$

Table 2. Amount of anthocyanidins in the samples.

S/N	Anthocyanidin	TCE (mg/100 g)	TCP (mg/100 g)
1	Pelargonidin (Pg)	4.148	2.250
2	Delphinidin (Dp)	535.313	563.365
3	Cyanidin (Cy)	72.700	43.817
4	Petunidin (Pt)	1.826	0.837
5	Peonidin (Pn)	1.223	0.121
6	Malvidin (Mv)	1.217	0.034
7	Total	616.426	610.423

current-voltage curves for the extracts of *T. catappa* are shown. The curves have the shapes of a typical I-V (shown as Figure 7) characteristic curve for DSSC. The TCP-TiO₂ sensitized cell has better photovoltaic properties than the TCE-TiO₂ sensitized cell.

In Figures 4 to 6, the photovoltaic curves of solar cells fabricated using pelargonidin, cyanidin and delphinidin as

sensitizers are shown, respectively. From these curves, when compared with a typical current-voltage curve for dye sensitized solar cell (Figure 7); the fill factors increased with purity of the compounds. However, delphinidin with highest percentages in the extracts has the least values in terms of photovoltaic performances.

In Table 3, the photovoltaic performances are shown

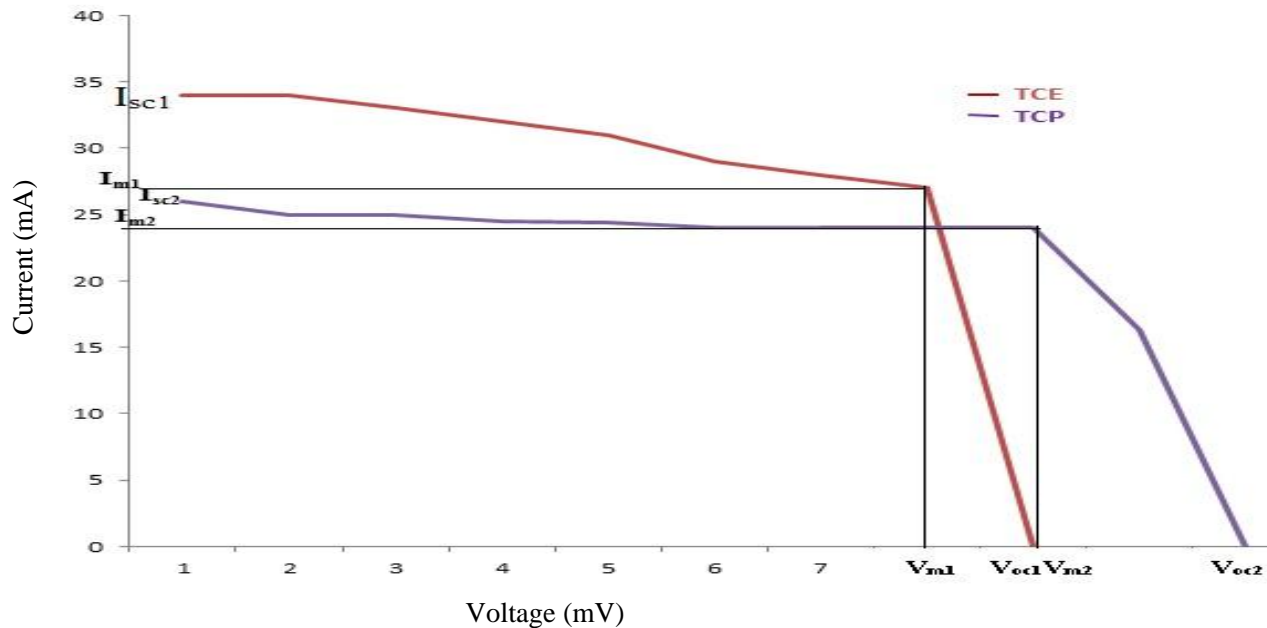


Figure 3. Current-voltage curve of solar cells fabricated using crude and purified extracts of *T. catappa* as sensitizers. I_{sc1} = Short circuit current for TCP; I_{sc2} = Short circuit current for TCP; I_{m1} = Maximum short circuit current for TCE; I_{m2} = Maximum short circuit current for TCP; V_{oc1} = Open circuit voltage for TCE; V_{oc2} = Open circuit voltage for TCP; V_{m1} = Maximum open circuit voltage for TCE; V_{m2} = Maximum open circuit voltage for TCP.

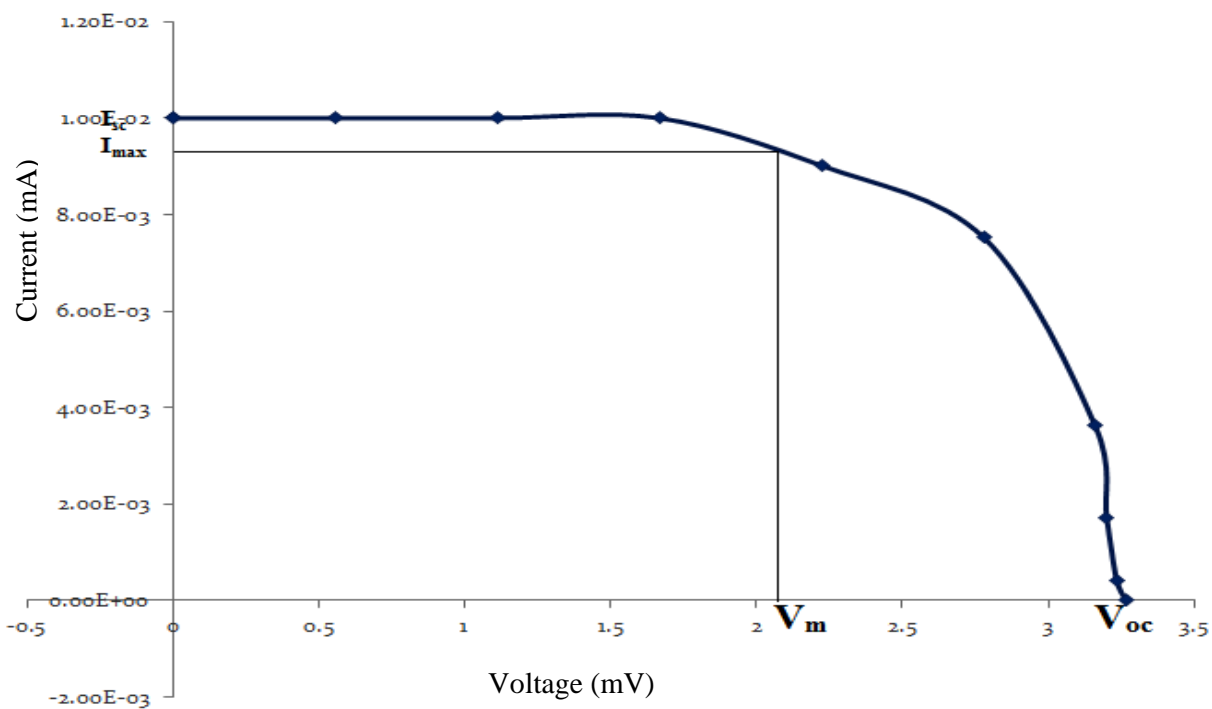


Figure 4. Pg: Current-voltage curve for solar cell using Pelargonidin as sensitizer.

for the crude (TCE), purified (TCP), extracts and three of the pure compounds (pelargonidin (Pg), cyanidin (Cy)

and delphinidin (Dp)). The photovoltaic graph for the $Mv-TiO_2$ was linear, rather than a curve. It showed deviation

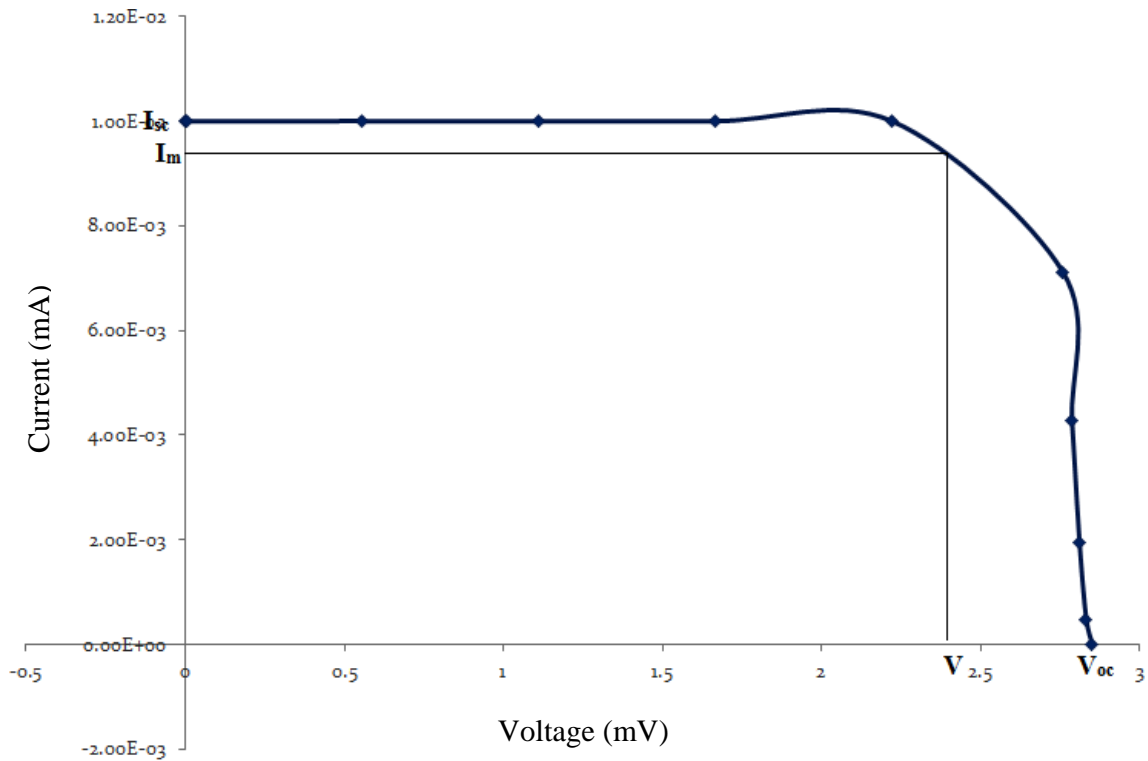


Figure 5. Current-voltage curve for solar cell using Cyanidin as sensitizer.

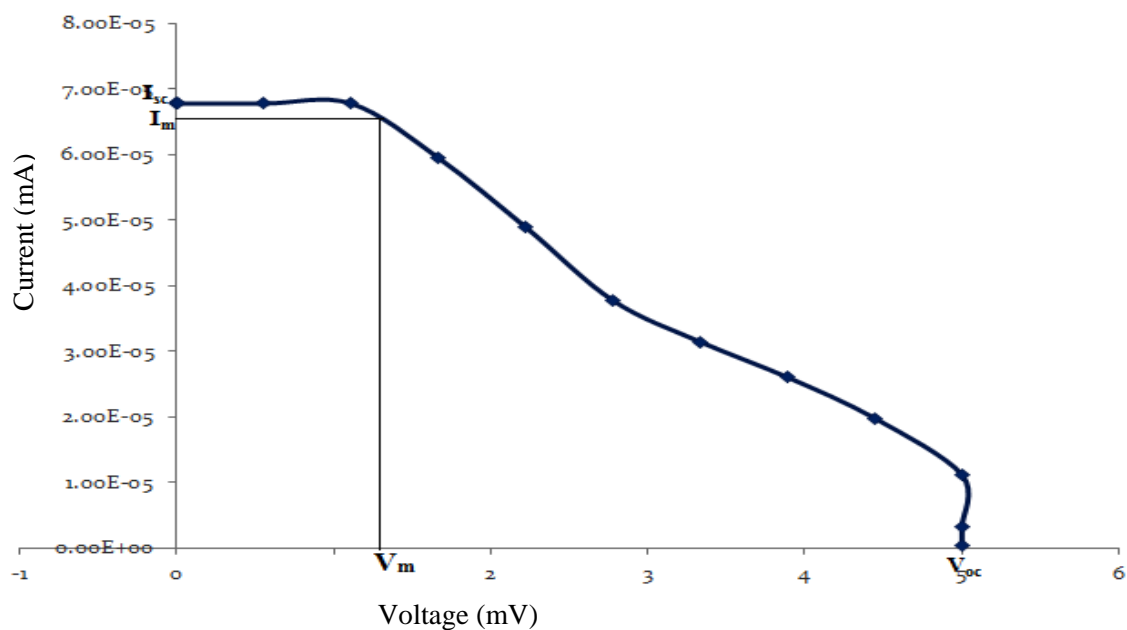


Figure 6. Current-voltage curve for solar cell using Delphinidin as sensitizer.

from the others.

The photovoltaic performance of the extracts and purified extracts of the samples applied as sensitizers in

DSCCs, it is evident from these data that the purified sample has higher fill factor and efficiency than the extracts.

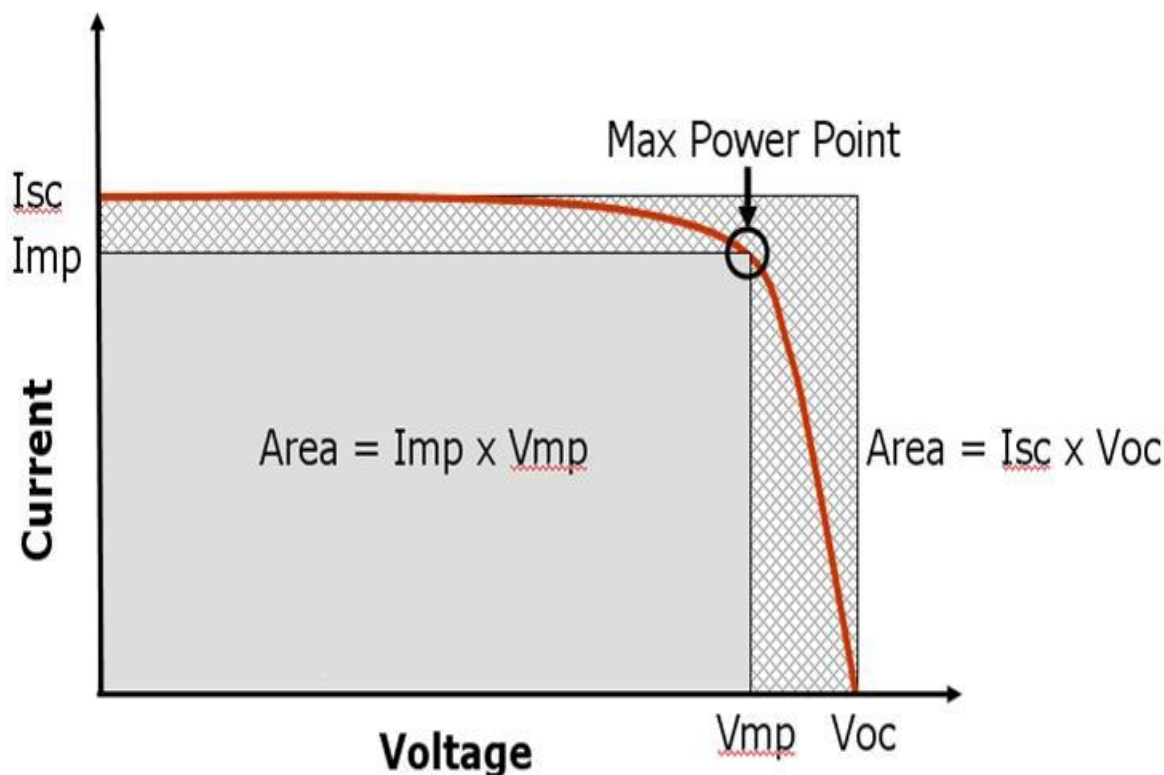


Figure 7. Typical current-voltage curve for dye sensitized solar cell; the Fill Factor is defined as the ratio of the two areas ($Area_1/Area_2$) (Boyo et al., 2012).

Table 3. Photovoltaic performance of the samples.

Sample	I_{sc} (mA)	J_{sc} (mA/cm ²)	V_{oc} (mV)	I_m (mA)	J_m (mA/cm ²)	V_m (mV)	FF	η (%)
TCE	0.037	0.009	25.000	0.016	0.004	10.500	0.280	0.336
TCP	0.027	0.007	27.000	0.025	0.006	14.920	0.493	0.746
Pg	1.100	0.278	31.200	1.010	0.250	28.600	0.826	1.43
Cy	1.130	0.283	48.200	1.020	0.255	44.500	0.835	2.27
Dp	0.068	0.017	26.89	0.068	0.017	11.12	0.415	0.004

Conclusion

The analysis of six common anthocyanins in the extract obtained from the calyxes of *T. catappa* was reported with delphinidin being the most abundant and its content increased with purification of the extract. DSSCs were constructed using the extracts of the withered leaves of *T. catappa*. The cell efficiencies increased with purity, with the best efficiencies of 2.27% for the Cy-sensitized TiO₂ cell.

The low efficiencies of the cells fabricated with TCE and TCP as sensitizers. These may be connected to the inhibitory effects of the composite anthocyanin (and other) molecules in the extracts. They reduce the sensitizing capability of the dyes to have low injection

efficiencies. Thereby, making the overlap of the dye excited states and the metal oxide conduction band, the dye regeneration kinetics and the dye excited state lifetime were not optimal. In order to enhance cell performance isolated compounds should be employed instead of the direct applications of the extracts.


Conflict of Interests

The authors have not declared any conflict of interests.

REFERENCES

Adenike B, Okafor P, Ibrahim A, Oluwole S, Boyo H (2013). Application

- of *Terminalia catappa* and leaves of *Azadirachta indica* calyxes as sensitizers in Dye-sensitized solar cells. *Int. J. Eng. Res. Dev.* 8(12):38-42.
- Andre SP, Neyde YMI (2006). Blue sensitizers for solar cells: Natural dyes from Calafate and Jaboticaba. *Solar Energy Mater. Solar Cells* 90:1936-1944.
- Bisquert J, Cahen D, Hodes G, Rühle S, Zaban A (2004). Physical Chemical Principles of Photovoltaic Conversion with Nanoparticulate, Mesoporous Dye-Sensitized Solar Cells. *J. Phys. Chem. B.* 108:8106-8119.
- Bisquert J, Palomares E, Quiñones C (2006). Effect of Energy Disorder in Interfacial Kinetics of Dye-Sensitized Solar Cells with Organic Hole Transport Material. *J. Phys. Chem. B.* 110:19406-19411.
- Boyo AO, Boyo HO, Abdulsalami IO, Adeola S (2012). Dye sensitized nanocrystalline titania solar cell using laali stem bark (*lawsonia inermis*). *Transnational J. Sci. Technol.* 2(4):60-72.
- Boyo AO, Okafor P, Abdulsalami IO, Oluwole S, Boyo HO (2013). Application of *Terminalia catappa* and leaves of *Azadirachta indica* calyxes as sensitizers in Dye-sensitized solar cells. *Int. J. Eng. Res. Dev.* 8(12):38-42.
- Brouillard R, Chassaing S, Fougerousse A (2003). Why are grape/fresh wine anthocyanins so simple and why is it that red wine color lasts so long? *Phytochemistry* 64:1179-1182.
- Chen MC, Liaw DJ, Huang CY, Wu HY, Tai NY (2011). Improving the efficiency of organic solar cell with a novel amphipolar polymer to form ternary cascade structure. *Solar Energy Mater. Solar cells.* 95:2621-2627.
- Close DC, Beadle CL (2003). The ecophysiology of foliar anthocyanin. *Bot. Rev.* 69:149.
- Duthie GG, Duthie SJ, Kyle JAM (2000). Plant polyphenols in cancer and heart disease: implications as nutritional antioxidants. *Nut. Res. Rev.* 13:79-88.
- Fossen T, Rayyan S, Andersen ØM (2004). Dimeric anthocyanins from strawberry (*Fragaria ananassa*) consisting of pelargonidin 3-glucoside covalently linked to four flavan-3-ols. *Phytochemistry* 65:1421-1430.
- Grätzel M (2004). Conversion of sunlight to electric power by nanocrystalline dye-sensitized solar cells. *J. Photochem. Photobiol. A: Chem.* 164:3-14.
- Harborne JB, Williams CA (2000). Advances in flavonoid research since 1992. *Phytochemistry* 55:481-493.
- Hwan KK, Dong HL, Myung JL, Hae MS, Bok JS, Kang DS, Mariachaiara P, Chiara A, Simona F, Filippo DA, Nazeeruddin Md, Grätzel M (2011). Organic dyes incorporating low-band-gap chromophores based on p-extended benzothiadiazole for dye-sensitized solar cells. *Dyes pigments* 91:192-198.
- Jordheim M, Fossen T, Andersen ØM (2006). Characterization of hemiacetal forms of anthocyanidin 3-O-β-glycopyranosides. *J. Agric. Food Chem.* 54:9340-9346.
- Kalaignan GP, Kang Y.S (2006). A review on mass transport in dye-sensitized nanocrystalline solar cells. *J. Photochem. Photobiol. C: Photochem. Rev.* 7(1):17-22.
- Kay A, Grätzel M (2002). Dye-Sensitized Core-Shell Nanocrystals: Improved Efficiency of mesoporous Tin Oxide Electrodes Coated with a thin layer of an Insulating Oxide. *Chem. Mater.* 14:29-30.
- Kelly CA, Meyer GJ (2001). Excited state processes at sensitized nanocrystalline thin film semiconductor interfaces. *Coordination Chem. Rev.* 211:295-304.
- Kim SS, Yum JH, Sung YE (2003). Improved performance of a dye-sensitized solar cell using a TiO₂/ZnO/Eosin Y electrode. *Solar Energy Mater. Solar Cells.* 79:495-507.
- Middleton EJ, Kandaswami C, Theoharides TC (2000). The effects of plant flavonoids on mammalian cells: implications for inflammation, heart disease and cancer. *Pharmacol. Rev.* 52:673-682.
- Poorman S, Mehra RM (2007). Effect of electrolytes on the photovoltaic performance of a hybrid dye ZnO solar cell. *Solar Energy Mater. Solar Cells* 91:518-524.
- Simmonds MSJ (2003). Flavonoid-insect interactions: recent advances in our knowledge. *Phytochemistry* 64:21.
- Takeda K, Sato S, Kobayashi H, Kanaitzuka V, Uene M, Kinoshita T (1994). The anthocyanin responsible for purplish blue flower colour of *Aconitum chinense*. *Phytochemistry* 36:613-616.
- Taofeek OA, Nasir AS, Musa TY, Adenike TO, Musbau AA, Joseph IO (2011). Antioxidant and drug detoxification potentials of *Terminalia catappa* anthocyanin extract. *Drug Chem. Toxicol.* 34(2):109-115.
- Wang P, Zakeeruddin S, Grätzel M (2010). High Efficiency solid-state sensitized heterojunction photovoltaic device. *Nano Today* 5:169-174.



International Journal of Physical Sciences

Related Journals Published by Academic Journals

- *African Journal of Pure and Applied Chemistry*
- *Journal of Internet and Information Systems*
- *Journal of Geology and Mining Research*
- *Journal of Oceanography and Marine Science*
- *Journal of Environmental Chemistry and Ecotoxicology*
- *Journal of Petroleum Technology and Alternative Fuels*

academicJournals